



High-resolution HO₂ radical detection by optical feedback linear cavity-enhanced absorption spectroscopy

Yang Chen^{1,2} · Nana Yang¹ · Bo Fang¹ · Weixiong Zhao¹ · Weijun Zhang^{1,2} · Shuangshuang Li^{1,2} · Weihua Cui¹

Received: 1 March 2024 / Accepted: 15 July 2024 / Published online: 24 July 2024
© The Author(s), under exclusive licence to Springer-Verlag GmbH Germany, part of Springer Nature 2024

Abstract

We report the development of an optical feedback linear cavity-enhanced absorption spectroscopy instrument for HO₂ detection using a distributed feedback (DFB) diode laser operating at 1506 nm. A direct and accurate method of reflectivity measurement based on the analysis of cavity mode signals was proposed. A differential circuit was used to judge the zero crossing point of the optical feedback cavity mode in the center of the frequency locking region, and shift the laser operating current to the non-resonant region. In this way, a ring-down signal was obtained with a time of 17.9 μs, corresponding to an effective absorption pathlength of 5.37 km. Combining the standing wave condition, the relationship between cavity length and drive voltage of the PZT mounted on the cavity rear mirror is translated into a correlation between the transmitted light wavenumber and the PZT voltage. The spectral resolution was improved from 290 MHz to 97 MHz by precisely tuning the PZT voltage. The achieved detection sensitivity of the system was $7 \times 10^{-10} \text{ cm}^{-1}$ with a data acquisition time of 10.6 s. The absorption spectrum of HO₂ at 6638.205 cm^{-1} was measured at a cell pressure of 50 mbar with a detection limit of $3.24 \times 10^9 \text{ molecule/cm}^3$.

1 Introduction

Laser absorption spectroscopy is widely used in trace gas detection owing to its advantages of non-destructive, high selectivity, high sensitivity, and rapid time response [1, 2]. Combined with a high finesse resonant cavity, the sensitivity can be significantly enhanced [3]. Optical feedback cavity-enhanced absorption spectroscopy (OF-CEAS) is a powerful tool for atmospheric measurement. The light leaking from the cavity directly return to the laser as seed light, which can improve its competitive advantage in the laser resonator and thus significantly reduce the laser phase and amplitude noise [4, 5]. OF-CEAS was first proposed by

Morville in 2005 [5] and has since been extensively applied in the field of environmental monitoring [6–10], isotope measurements [11–13], and scientific investigations [14, 15].

The detection limit of absorption spectroscopy closely related to the optical path [3]. It is very important to accurately measure the reflectivity of the cavity mirror in OF-CEAS. In recent years, there are two main methods for determining the mirror reflectivity. The first method is to use a calibrated gas with a known concentration to get the cavity mirror reflectivity [10]. However, this method requires a suitable standard gas in the absorption band, and the accuracy of the result also depends on the accuracy of the standard gas concentration. The other method is ring-down measurement, which is simple, highly sensitive and accurate [16]. The ring-down event can be achieved by switching off the laser, and then the reflectivity of the cavity mirror can be obtained by calculating the ring-down time.

There are several different ways to achieve the ring-down event. In the first method, the laser is suddenly switched off the laser at the top of a preselected cavity mode to trigger the ring-down event. The acquisition program periodically records the ring-down time to ensure that the change in reflectivity is updated in real time. A timer card is used to select the exact instant when the ring-down should occur

✉ Nana Yang
nanayang@aiofm.ac.cn

✉ Weixiong Zhao
wxzhao@aiofm.ac.cn

¹ Laboratory of Atmospheric Physico-Chemistry, Anhui Institute of Optics and Fine Mechanics, Hefei Institutes of Physical Science, Chinese Academy of Sciences, Hefei 230031, China

² University of Science and Technology of China, Hefei 230026, China

in the scan [6, 11, 17]. The second method is to switch off the laser in the last mode by adding a negative square wave signal to the swept injection current [18, 19]. This method allows for a more intuitive selection of the ring-down position, but precise control of the swept injection current is critical to ensure that the ring-down event occurs within the last mode range. The third method is to obtain the ring-down time by using the pulse signal to cut off the laser current when the cavity resonance is detected [13, 20]. In addition to the above methods, there is a laser beam shut-down scheme in which the ring-down occurs at the trailing edge of the rounded peak of the cavity mode [21]. Since the ring-down event occurs at the boundary of the locking range, the laser off-state duration is limited by the laser thermal inertia and cavity mode interval.

The spectral resolution is also a crucial parameter in spectral measurement. For OF-CEAS, the spectral resolution is inherently limited by the free spectral range (FSR) of the resonant cavity. When measurement is performed at lower pressure, the spectrum contains fewer data points, which greatly limits the accuracy of concentration retrieval [5]. Therefore, increasing the spectral resolution of OF-CEAS is the key to improving the accuracy of the system.

In this paper, a high spectral resolution OF-CEAS technique based on in-situ measurement of reflectivity was presented. The center position of the cavity mode was automatically identified by differentiating the cavity output signal and set as the trigger signal to control the decay event. The operating current translation makes the laser far away from the resonant position via the TTL signal, which leads to the ring-down event occurring at the center of the locking range. Additionally, the cavity length is precisely modulated using a piezoelectric transducer (PZT) mounted on the end mirror of the cavity, enabling the acquisition of more data points per frequency unit and achieving high line shape precision. Finally, the instrument was applied to the high-resolution measurement of HO₂ radical at 6638.205 cm⁻¹.

2 Theory

Optical feedback (OF) is a self-injection locking technique that can greatly improve the laser-cavity coupling. Currently, there are two types of resonant cavity in optical feedback: V-shaped cavity [20–22] and linear cavity [23–26]. The V-shaped cavity can separate the resonant light from the non-resonant light, ensuring that only the resonant light returns to the laser, which can achieve a more robust laser locking. However, the folding mirror has slightly different effects on odd mode and even mode, resulting in two groups of distribution of the cavity modes [4]. Compared to the V-shaped cavity, the linear cavity has a simpler structure,

avoids the odd-even mode problem, and provides higher cavity finesse under the same mirror reflectivity. The linear cavity cannot avoid the non-resonant light returning to the laser, but the effect of the non-resonant light can be reduced by adjusting the phase reasonably. In this paper, the linear cavity OF-CEAS technique is adopted for research.

In the case of weak feedback, the rate equation that describes the evolution of the electric field amplitude versus time at the laser output facet for a linear cavity is given by [22–26]:

$$\frac{d(E(t)e^{i(\omega t + \phi(t))})}{dt} = [i\omega_{free} + \frac{1}{2}(G(n) - \Gamma)(1 + i\alpha)] E(t)e^{i(\omega t + \phi(t))} + \sum_{m=0}^{\infty} K_1 E(t - \tau_m) e^{i(\omega(t - \tau_m) + \phi(t - \tau_m))} - K_2 E(t - \tau_n) e^{i(\omega(t - \tau_n) + \phi(t - \tau_n))} \tag{1}$$

where ω is the coupled laser angular frequency, ω_{free} is the free-running laser angular frequency, ϕ is the laser output phase, G is the net rate of stimulated emission, Γ is the photon decay rate, and α is Henry factor. In addition, τ_m is the time for the photon to travel from the laser to the cavity and back to the laser after m round trips in the cavity, and τ_n is the round-trip time of the photon between the laser and the cavity front mirror. The first item on the right side of Eq. (1) is the case without feedback, while the second and the third terms are introduced by optical feedback from resonant and non-resonant light respectively. The feedback coupling coefficient of resonant and non-resonant light can be expressed as [22]:

$$K_1 = \frac{c}{2\eta l_a} \sqrt{\beta} \frac{1 - r_0^2}{r_0} r (1 - r^2) (r^2)^m \tag{2}$$

$$K_2 = \frac{c}{2\eta l_a} \sqrt{\beta'} \frac{1 - r_0^2}{r_0} r \tag{3}$$

where η is the refractive index of the medium in the laser cavity, l_a is the length of the laser cavity, β is the feedback rate of the resonant light, and β' is the feedback rate of the non-resonant light. The feedback rates were set within the reasonable range based on the literatures ($\beta = 1.8 \times 10^{-5}$, $\beta' = 3 \times 10^{-6}$) [4, 10, 24].

Therefore, the relationship between the free-running laser frequency and the coupled laser frequency can be written as [22, 24]:

$$\omega_{free} = \omega + \frac{c\sqrt{\beta(1+\alpha^2)} \frac{F_{cav}}{2\eta l_a} \frac{F_{DL}}{F_{DL}}}{\sin[\frac{2\omega}{c}(\eta l_a + l_b + l_c) + \theta] - r^2 \sin[\frac{2\omega}{c}(\eta l_a + l_b) + \theta]} \frac{1 + (\frac{2F_{cav}}{\pi})^2 \sin^2[\frac{\omega}{c} l_c]}{1 + (\frac{2F_{cav}}{\pi})^2 \sin^2[\frac{\omega}{c} l_c]} - \frac{\pi r c \sqrt{\beta'(1+\alpha^2)}}{2\eta l_a F_{DL}} \sin[\frac{2\omega}{c}(\eta l_a + l_b) + \theta] \tag{4}$$

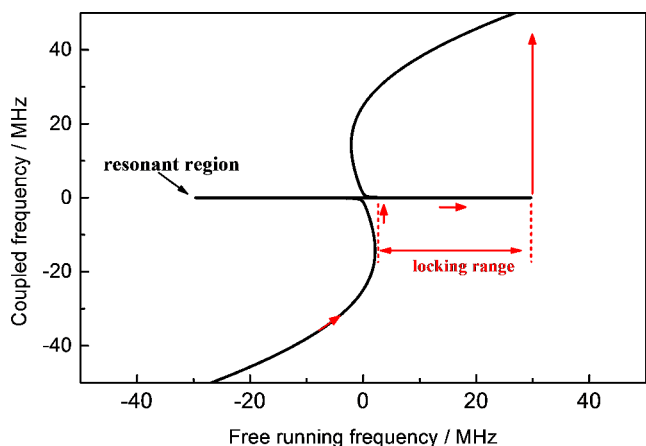


Fig. 1 Response of laser coupling frequency at the resonance point under linear cavity optical feedback

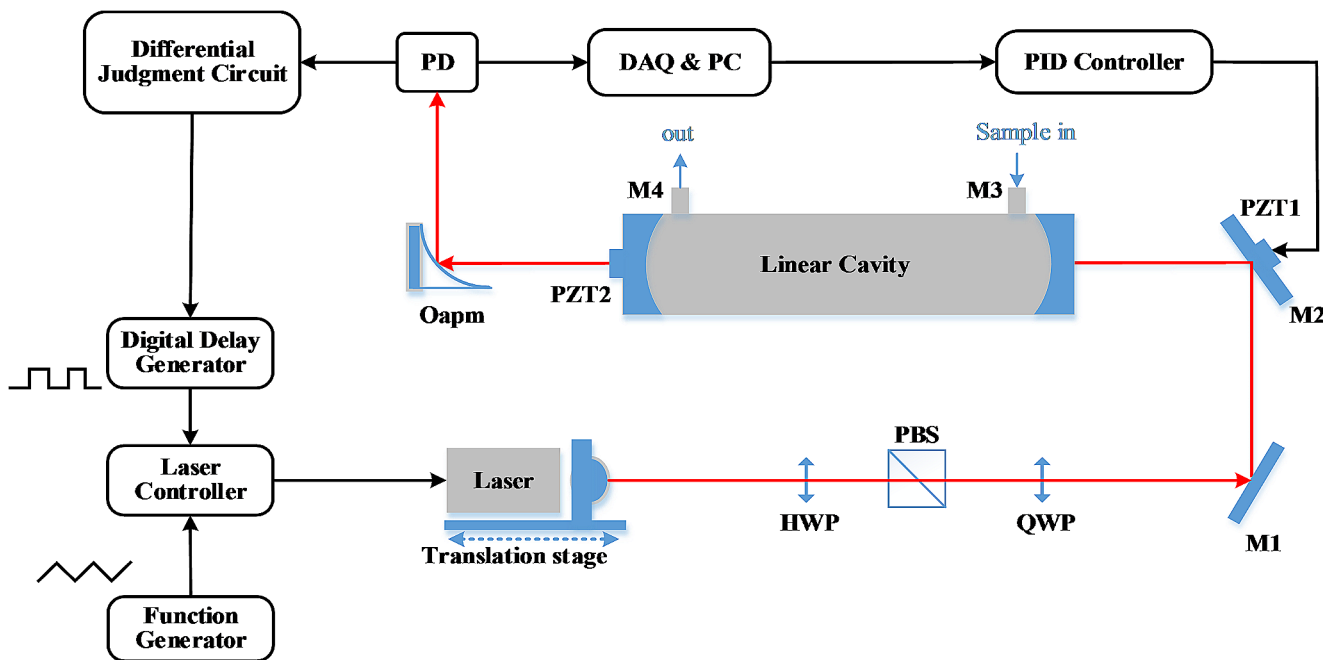
where l_b and l_c are the distance from the laser to the resonator and the length of the resonator respectively. $F_{cav} = \frac{\pi r}{1-r^2}$ and $F_{DL} = \frac{\pi r_0}{1-r_0^2}$ are the finesse of the cavity and the laser cavity, respectively.

The simulation of the coupled laser frequency calculated using Eq. (4) was shown in Fig. 1. When the laser frequency is close to the resonance region, it can lock to the external high-finesse cavity. However, the frequency will jump during the locking process due to the laser frequency

monotonically tuning. The arrows in Fig. 1 represent the actual response of the laser, and the flat part between the two frequency jumps is defined as the locking range.

3 Experimental section

The experimental setup of the linear OF-CEAS instrument for HO₂ detection is depicted in Fig. 2. The laser source used was a DFB diode laser (NTT Electronics, NLK1S5EAYF) operating at 1506 nm with a typical output power of ~ 10 mW and a linewidth of ~ 2 MHz. The temperature and current of the laser are controlled by the laser controller (Stanford Research, LDC501). Frequency tuning was achieved by scanning the injection current with a ramp generated by a function generator (Keysight, 33600 A). The laser was mounted on a self-made aluminum mount and then put them on a precision translation stage for back and forth movements. The output of the laser is collimated by a collimating lens (Thorlabs, C330TMD-C) and then passes through, in sequence, a half-wave plate (Lbtek, HWP20-1550BM), a polarization beam splitter (Lbtek, MPBS24-1550) cube, a quarter-wave plate (Thorlabs, WPQ05M-1550) and two mirrors. Then it couples into the high-finesse linear optical cavity, which is formed by two high-reflectivity mirrors



- HWP: half wave plate;
- PZT: piezoceramics;
- PD: photodetector;
- Oapm: off-axis parabolic mirror
- QWP: quarter wave plate;
- M1, M2: plane mirrors;
- PC: personal computer;
- PBS: polarization beam splitter;
- M3, M4: high reflectivity mirrors;
- DAQ: data acquisition;

Fig. 2 Experimental setup of the linear OF-CEAS instrument

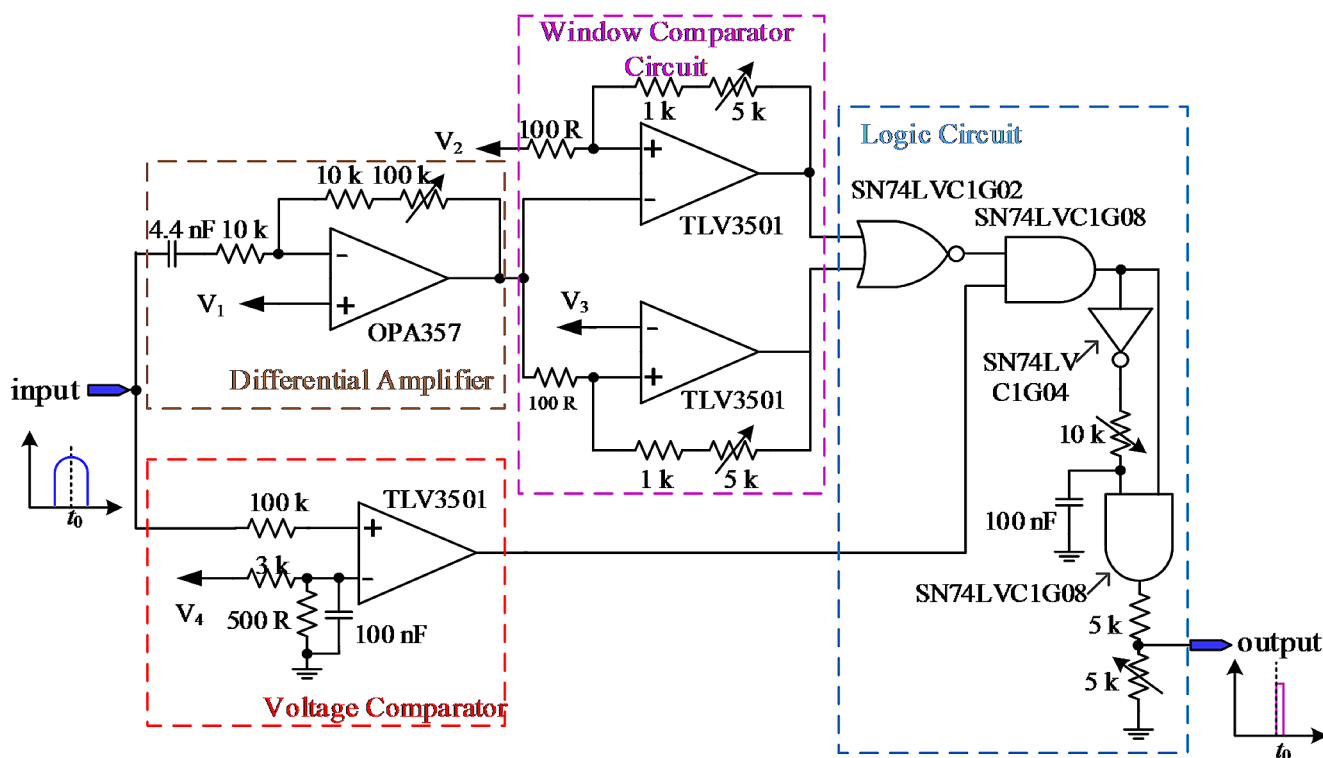
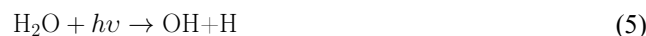


Fig. 3 Principle of the differential judgment circuit

($R > 99.99\%$) installed in mirror chambers and protected with flushed pure N_2 . The cavity length is 51.8 cm, indicating a FSR of 290 MHz. The rear mirror of the cavity (M4) was fitted with a piezoelectric ring chip PZT2 (Thorlabs, PK44M3B8P2) for tuning the cavity length. Both ends of the cavity are sealed by two wedge windows (Thorlabs, WW71050-D). The transmitted beam was focused by a 90° off-axis parabolic mirror onto an InGaAs avalanche photodetector (Thorlabs, APD410C). The output of the photodetector is used to control the PZT1 (Thorlabs, PA44M3KW) on the mirror M2 through PID feedback to achieve precise tuning of the distance between the laser and the cavity. And the signal was also used for accessing the differential judgment circuit for cavity mirror reflectivity measurement. The flow rate of the sample was controlled by a mass flow meter (Sevenstar Electronics, CS-200). The pressure of the cavity was maintained at 50 mbar with an electric butterfly valve (VAT DN40KF). The entire experimental setup was installed in a $1000 \times 400 \times 140 \text{ mm}^3$ duralumin chassis to maintain mechanical stability.

Due to the high reactivity and oxidation of HO_2 radicals, the inlet was as short as possible to reduce loss. The optical cavity was made of a perfluoroalkoxy (PFA) tube with 9 mm inner diameter and 12.7 mm outer diameter. The cavity and pipes are connected by PFA tee unions (Swagelok). To continuously generate HO_2 radicals, a custom-built photochemical reactor was used [27]. The reactor consists of a 300 mm

long quartz tube with an external diameter of 160 mm and a wall thickness of 3 mm, in the center of which are mounted two low-pressure Hg lamps (Analytic Jena, 90–0004) with a wavelength of 184.9 nm. The HO_2 was produced by photolysis of water vapor:



To prevent overheating of the Hg lamp and reduce the production of O_3 during the reaction, a small amount of N_2 was used to cool the Hg lamps.

4 Mirror reflectivity measurement based on differential judgment circuit

To achieve high accurate measurement of the mirror reflectivity, the ring-down event should occur within the locking range. Therefore, a scheme based on optical feedback cavity mode signal analysis was proposed. A self-designed differential judgment circuit is used to identify the zero-crossing point of the derivative signal (the center of the locking range) and trigger optical ring-down. The advantages of this method: (1) When the frequency is located at the center of the lock range, it achieves the optimal frequency coupling

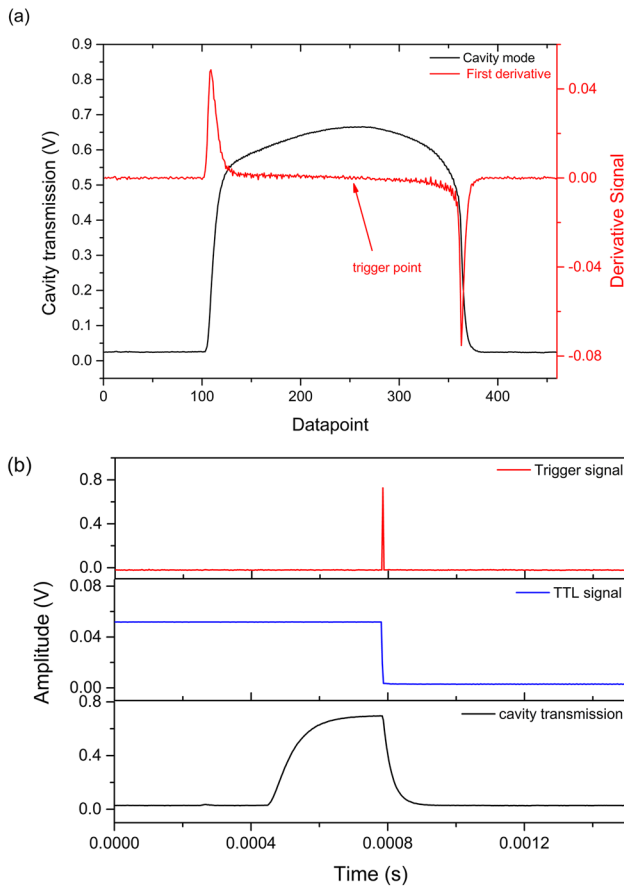


Fig. 4 (a) Signals of cavity mode and its differentiation; (b) The time sequence of the ring-down process signals

efficiency. (2) Because the frequency jump point is not very easy to identify on the mode signal, especially for narrow modes. If the decay event triggered at other points away from the center point, it is likely to exceed the locking range. (3) There is no need to set a threshold value, as the circuit can automatically determine the ring-down moment, which simplifies the CRDS measurement steps and eliminates the use of device such as AOM.

The principle of the differential judgment circuit was shown in Fig. 3. The circuit is composed of a derivative circuit, a window comparison circuit, a voltage comparator, and a logic circuit. The input signal is subjected to differentiation to generate its first-order derivative, and then processed by a window comparison circuit to detect the zero-crossing point. To avoid interference from non-target signals, especially zero-level signals outside the cavity mode, the logic verification process is introduced. Through the voltage comparison unit, the detected signal is compared with the cavity mode signal to identify the correct zero-crossing. After confirmation, the logic circuit outputs a high-level signal. This signal acts as a trigger signal for ring-down measurement. The trigger signal was input to the digital delay pulse

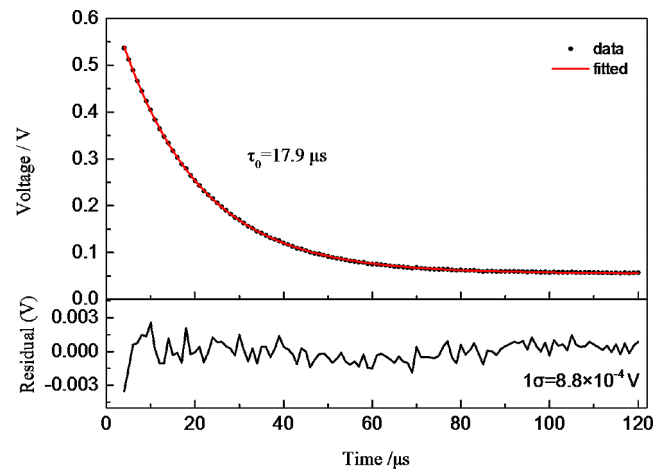


Fig. 5 Cavity ring-down signal and its fitting residual

generator (DG645) to generate a TTL signal. When the high level of the TTL signal was triggered into a low level, the laser current will shift slightly to move the cavity mode to the non-resonant region, thus generating a ring-down signal. The cavity mode and its first derivative were shown in Fig. 4(a), and signals in the trigger ring-down process were shown in Fig. 4(b).

The fitting results of the ring-down signal were shown in Fig. 5. The ring down time is $\tau_0 = 17.9 \mu\text{s}$, corresponding to the cavity finesse of $\sim 31,000$, and the pathlength of $\sim 5.37 \text{ km}$.

5 Results and discussion

5.1 Control of feedback phase and feedback rate

In optical feedback, the stringent constraint on feedback phase is indispensable. To ensure that all the cavity modes satisfy the phase condition, the laser-to-cavity distance needs to be controlled to be an integer multiple of the cavity length. When feedback phase is in an optimum condition, the cavity transmission signal is symmetrical, otherwise it will be deformed [5]. Figure 6(a) is the experimental transmission signals under different phase conditions. The laser was mounted on a precision translation stage to achieve rough adjustment of the distance. Then, fine distance adjustment was realized via the PZT1 mounted on the steering mirror M2. An electronic servo loop (implemented based on LabVIEW program) maintained the correct phase based on cavity mode symmetry analysis [10].

The OF rates affect the locking range [5]. In the process of the experiment, the values of the feedback rates does not need to be precisely known. By adjusting the feedback rate control unit (half-wave plate, polarizing beam splitter cube, and quarter-wave plate), the cavity mode signal can

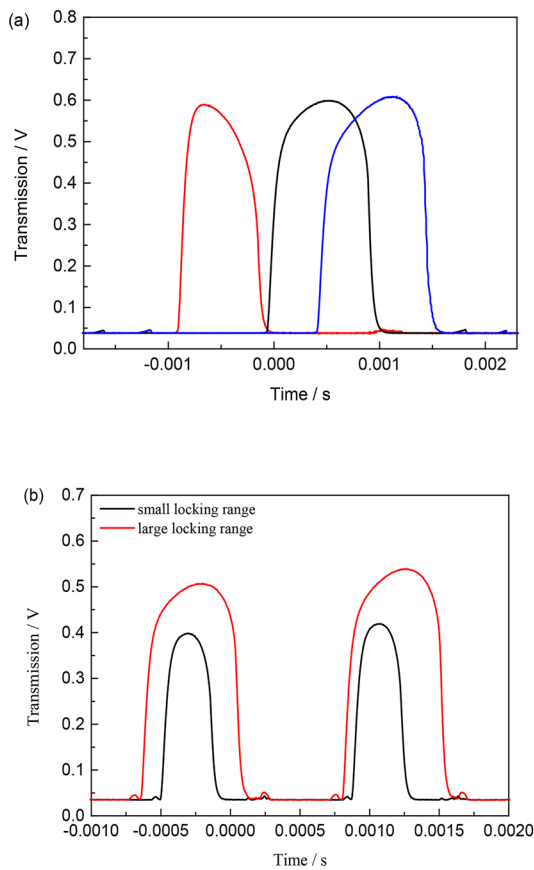


Fig. 6 The experimental transmission signals (a) under different phase conditions and (b) at different feedback rates

be optimized to achieve better experimental conditions. Figure 6(b) shows the cavity transmission signals at different feedback rates in the experiment.

5.2 High spectral resolution OF-CEAS spectrum

The spacing of data points in a typical OF-CEAS spectrum is perfectly regular and amounts to about 290 MHz (FSR of the cavity) when the cavity length is fixed. A low number of points across a molecular absorption feature may lead to difficulties in precisely fitting the line-shape profile, which has consequences for precisely determining the concentration. According to the equation of FSR ($FSR = c/2nl_c$, l_c is

the cavity length), the longer cavity length has the smaller FSR. But excessively increasing the cavity length will make the instrument larger and less stable. Due to the frequency selectivity of the cavity, only the frequency of the light satisfied the standing wave condition ($l_c = q \times \lambda/2n$, q is the ordinal number of the longitudinal mode, n is the refractive index of the medium) can transmit stably. Therefore, transmitted light of different frequencies can be obtained by slightly adjusting the cavity length l_c , thus overcoming the spectral resolution limitation caused by FSR. The principle of frequency selection of F-P cavity was shown in Fig. 7.

The tuning of the cavity length was realized by PZT2 tuning mounted on the cavity mirror M4. The relationship between displacement y and drive voltage x of PZT2 can be obtained from the specification provided by the manufacturer:

$$y = -0.24 + 0.18x - 5.99 \times 10^{-4}x^2 + 6.59 \times 10^{-7}x^3 \quad (7)$$

Combined with the standing wave condition, Eq. 7 can be converted into the relationship between the wavenumber of transmitted light and voltage. Thus the transmission frequency can be controlled more intuitively. By selecting suitable voltages, a uniformly distributed interlaced spectrum can be attained.

The device employs an aluminum cavity, kept at constant pressure by a butterfly valve, and mounted on an optical breadboard for vibration isolation. The experimental temperature was kept constant. During a set of interlaced spectrum measurements lasting less than 10 min, the temperature fluctuation is less than 0.1°C. Using the thermal expansion coefficient of aluminum to calculate, the change in cavity length is less than 0.12 μm , and the corresponding frequency drift is less than 0.16 times of FSR near 6638.20 cm^{-1} . The effect of frequency drift is not considered in this experiment.

5.3 HO₂ absorption spectrum measurement

The HO₂ sample gas generated from the photochemical reactor was injected into the cavity at a flow rate of 0.8 L/min. The pressure inside the cavity was maintained at 50 mbar.

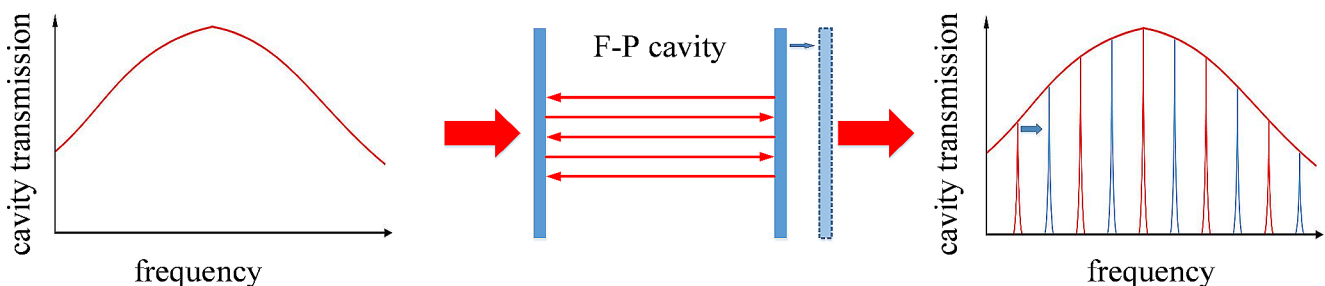


Fig. 7 Frequency selection of F-P cavity

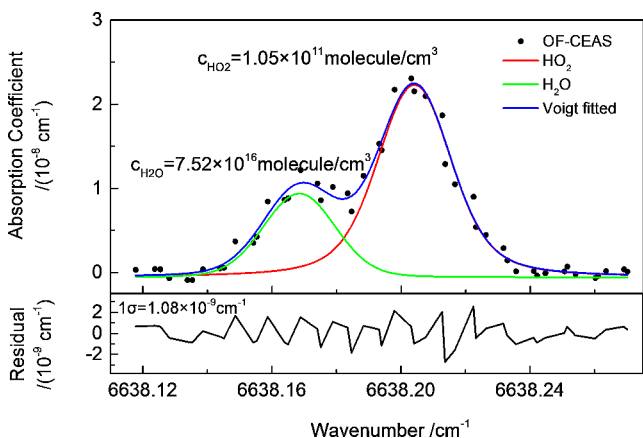


Fig. 8 Absorption spectrum of HO₂ and H₂O near 6638.20 cm⁻¹

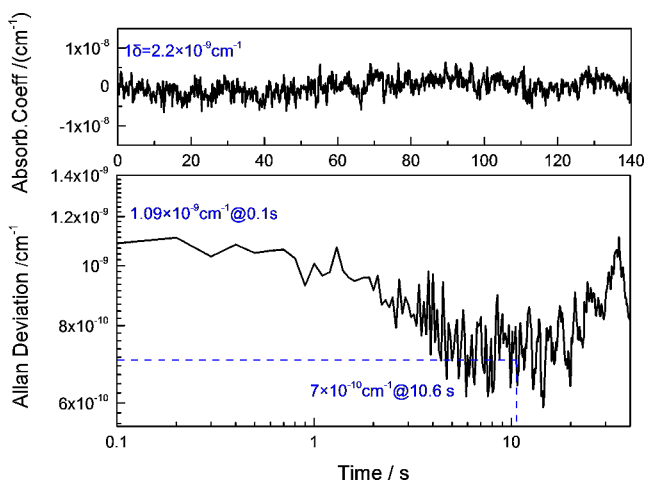


Fig. 9 Performance evaluation of the OF-CEAS instrument. Upper panel: time series measurement of absorption coefficient for a cavity mode. Lower panel: Allan deviation plot

The HO₂ absorption line with the strongest line intensity (6638.20 cm⁻¹, $S = 7.09 \times 10^{-21} \text{ cm}^{-1}/(\text{molecule cm}^{-2})$) currently known in the near-infrared band was selected for detection [28]. To obtain successive cavity modes, the laser current was scanned using a 50 Hz triangular wave. One of the modes was selected for the symmetry analysis. The difference between the left and right parts of the cavity mode was fed to the PID controller as an error signal to precisely control PZT1 to maintain the phase matching [10]. Then, we retrieve the amplitude of each cavity mode to obtain the absorption spectrum signal. The absorption coefficient α_{abs} can be written in the form [10]:

$$\alpha_{\text{abs}} = \frac{1}{l_c} \left(\sqrt{\frac{I_0}{I}} - 1 \right) (1 - R) \tag{8}$$

where I and I_0 are the transmission intensity with and without absorbing gas sample respectively.

The driving voltage of PZT2 was selected as 0 V, 16.34 V, and 33.47 V to get a spectrum with a uniform point distribution. The spectral resolution was enhanced from 290 MHz to 97 MHz. A Voigt line profile was used to fit the data with Levenberg–Marquardt non-linear least square method. The results were shown in Fig. 8. The concentration of HO₂ was determined to be $1.05 \times 10^{11} \text{ molecule/cm}^3$. With a fit residual of $1.08 \times 10^{-9} \text{ cm}^{-1}$ and the peak absorption of HO₂ radical of $2.25 \times 10^{-8} \text{ cm}^{-1}$, a 1σ detection limit of $\sim 5 \times 10^9 \text{ molecule/cm}^3$ was achieved. The Allan variance analysis (Fig. 9) shows that the detection sensitivity can be further improved to $7 \times 10^{-10} \text{ cm}^{-1}$ with an average time of 10.6 s, corresponding to a detection limit of $\sim 3.24 \times 10^9 \text{ molecule/cm}^3$ for HO₂ radical.

Currently, the highest sensitivity achieved with OF-CEAS technology was $8 \times 10^{-11} \text{ cm}^{-1}$ (0.5 s) with an effective optical pathlength of 90 km ($R = 99.9989\%$, $d = 97.8 \text{ cm}$) [29]. When comparing the minimal detectable fractional absorption ($\sim 7.2 \times 10^{-4}$), the results in this paper ($\sim 3.76 \times 10^{-4}$) are comparable. By enhancing the stability of the cavity, optimizing the performance of the phase servo loop, and employing cavity mirrors with higher reflectivity, the sensitivity of the system can be further improved.

The optical feedback technique has shown significant advantages in frequency stabilization and line width reduction. It has great significance for improving the performance and stability of the laser. At present, using the optical feedback effect to achieve narrow-linewidth and ultra-stable laser source has become a high-profile research direction [30, 31].

6 Conclusion

In this paper, we present the development of a linear high-resolution OF-CEAS instrument with a 1506 nm DFB diode laser for HO₂ radical detection. A self-designed differential judgment circuit was used to automatically determine the center of the frequency-locked region through the analysis of the optical feedback signal and sent a trigger signal to initiate ring-down event. By tuning the length of the cavity, more frequency light can be transmitted through the cavity, thereby improving the spectral resolution. A minimum detectable absorption coefficient of $7 \times 10^{-10} \text{ cm}^{-1}$ (10.6 s) was achieved, giving an HO₂ detection limit of $3.24 \times 10^9 \text{ molecule/cm}^3$ with a spectral resolution of 97 MHz at 6638.205 cm⁻¹. The instrument provides a simple and efficient method for the detection of HO₂ radical. Moreover, the narrow linewidth laser with stable frequency obtained by optical feedback can be used as a new light source, which can be combined with a variety of techniques for further research.

Author contributions YC: Conceptualization, Methodology, Investigation, Editing & data analysis, Writing-original draft, Writing-review & editing NY : Methodology, Writing-review & editing BF: Writing-review & editing , Funding acquisition WZ: Methodology, review and editing, Funding acquisition, Resources WZ: Methodology, Resources SL: Investigation WC: Investigation.

Funding National Natural Science Foundation of China (U21A2028), the Youth Innovation Promotion Association CAS (Y202089), and the HFIPS Director's Fund (BJPY2023A02, YZJJ202101).

Data availability No datasets were generated or analysed during the current study.

Declarations

Competing interests The authors declare no competing interests.

References

- Z. Du, S. Zhang, J. Li, N. Gao, K. Tong, *Appl. Sci.* **9**(2), 338 (2019)
- B. Fu, C. Zhang, W. Lyu, J. Sun, L. Xu, *Appl. Spectrosc. Rev.* **57**(2), 112–152 (2022)
- J. Hu, F. Wan, P. Wang, H. Ge, W. Chen, *Appl. Spectrosc. Rev.* **57**(5), 378–410 (2021)
- J. Morville, D. Romanini, E. Kerstel, *Cavity-Enhanced Spectrosc. Sens.* **179**, 163–209 (2014)
- J. Morville, S. Kassi, M. Chenevier, D. Romanini, *Appl. Phys. B* **80**, 1027–1038 (2005)
- D. Romanini, M. Chenevier, S. Kassi, M. Schmidt, C. Valant, M. Ramonet, J. Lopez, H.-J. Jost, *Appl. Phys. B* **83**, 659–667 (2006)
- S. Kassi, M. Chenevier, L. Gianfrani, A. Salhi, Y. Rouillard, A. Ouvrard, D. Romanini, *Opt. Express.* **14**(23), 11442–11452 (2006)
- G. Maisons, P. Gorrotxategi Carbajo, M. Carras, D. Romanini, *Opt. Lett.* **35**(21), 3607–3609 (2010)
- I. Ventrillard, I. Xueref-Remy, M. Schmidt, C. Yver Kwok, X. Faïn, Romanini, *Atmos. Meas. Tech.* **10**, 1803–1812 (2017)
- N. Yang, B. Fang, W. Zhao, C. Wang, F. Cheng, X. Hu, Y. Chen, W. Zhang, W. Ma, G. Zhao, W. Chen, *Opt. Express.* **30**(9), 15238–15249 (2022)
- E.R.T. Kerstel, R.Q. Iannone, M. Chenevier, S. Kassi, H.-J. Jost, D. Romanini, *Appl. Phys. B* **85**, 397–406 (2006)
- S.G. Baran, G. Hancock, R. Peverall, G.A.D. Ritchie, N.J. Van Leeuwen *Analyst.* **134**(2), 243–249 (2009)
- K. Jiao, J. Gao, J. Yang, G. Zhao, Z. Shi, X. Wang, D. Zhu, H. He, J. Qing, X. Yan, W. Ma, S. Jia, *Microw. Opt. Technol. Lett.* **66**, e33946 (2024)
- R. Grilli, N. Marrocco, T. Desbois, C. Guillermin, J. Triest, E. Kerstel, D. Romanini, *Rev. Sci. Instrum.* **85**, 111301 (2014)
- R. Grilli, J. Triest, J. Chappellaz, M. Calzas, T. Desbois, P. Jansson, C. Guillermin, B. Ferré, L. Lechevallier, V. Ledoux, D. Romanini, *Environ. Sci. Technol.* **52**, 10543–10551 (2018)
- S. Xiao, B. Li, J. Wang, *Metrologia.* **57**(5), 055002 (2020)
- P. Gorrotxategi-Carbajo, E. Fasci, I. Ventrillard, M. Carras, G. Maisons, D. Romanini, *Appl. Phys. B* **110**, 309–314 (2013)
- F. Wan, W. Chen, C. Gu, J. Zou, L. Du, W. Qi, Q. Zhou, *Spectrosc. Spectr. Anal.* **35**(10), 2792–2796 (2015). (in Chinese)
- I. Ventrillard, P. Gorrotxategi-Carbajo, D. Romanini, *Appl. Phys. B* **123**, 180 (2017)
- J. Yang, G. Zhao, J. Kang, J. Gao, X. Yan, Y. Zhao, W. Ma, S. Jia, *Acta Phys. Sin.* **73**(01), 199–206 (2024). (in Chinese)
- V. Motto-Ros, M. Durand, J. Morville, *Appl. Phys. B* **91**, 203–211 (2008)
- X. Wang, G. Zhao, K. Jiao, B. Chen, R. Kan, Z. Cong, J. Liu, W. Ma, *Front. Phys.* **10**, 857371 (2022)
- K.M. Manfred, L. Ciaffoni, G.A.D. Ritchie, *Appl. Phys. B* **120**, 329–339 (2015)
- J. Tian, G. Zhao, A.J. Fleisher, W. Ma, S. Jia, *Opt. Express.* **29**(17), 26831–26840 (2021)
- H. Ge, W. Kong, R. Kong, G. Wang, W. Zhao, W. Ma, F. Chen, W. Ma, *Opt. Lett.* **48**(8), 2186–2189 (2023)
- F. Wan, R. Wang, H. Ge, W. Kong, H. Sun, H. Wu, G. Zhao, W. Ma, W. Chen, *Opt. Express.* **32**(7), 12428–12437 (2024)
- C. Wang, W. Zhao, B. Fang, N. Yang, F. Cheng, X. Hu, Y. Chen, W. Zhang, C. Fittschen, W. Chen, *Opt. Express.* **30**(21), 37446–37456 (2022)
- N. Ibrahim, J. Thiebaud, J. Orphal, C. Fittschen, *J. Mol. Spectrosc.* **242**, 64–69 (2007)
- J. Landsberg, D. Romanini, E. Kerstel, *Opt. Lett.* **39**(7), 1795–1798 (2014)
- T. Ryohei, S. Keisuke, S. Volker, O. Yuki, I. Kazuki, M. Kazune, K. Yuta, F. Tetsuo, T. Koji, N. Shinichi, Y. Kenji, T. Hideki, *J. Appl. Phys.* **132**, 083102 (2022)
- J. Burkart, S. Kassi, *Appl. Phys. B* **119**, 97–109 (2015)

Publisher's Note Springer Nature remains neutral with regard to jurisdictional claims in published maps and institutional affiliations.

Springer Nature or its licensor (e.g. a society or other partner) holds exclusive rights to this article under a publishing agreement with the author(s) or other rightsholder(s); author self-archiving of the accepted manuscript version of this article is solely governed by the terms of such publishing agreement and applicable law.